Hindawi
Geofluids
Volume 2018, Article ID 7801843, 18 pages
https://doi.org/10.1155/2018/7801843

*Research Article*

# Mechanical-Chemical-Mineralogical Controls on Permeability Evolution of Shale Fractures

**Yunzhong Jia,[1,2] Yiyu Lu,[1] Jiren Tang,[1] Yi Fang,[2,3] Binwei Xia,[1] and Zhaolong Ge[1]**

[1]*State Key Laboratory for Coal Mine Disaster Dynamics and Control, Chongqing University, Chongqing 400044, China*
[2]*Department of Energy and Mineral Engineering, EMS Energy Institute, and G3 Center, The Pennsylvania State University, University Park, PA 16802, USA*
[3]*Institute for Geophysics, Jackson School of Geosciences, University of Texas at Austin, Austin, TX 78712, USA*

Correspondence should be addressed to Yiyu Lu; luyiyu@cqu.edu.cn and Jiren Tang; jrtang2010@163.com

Received 15 April 2018; Revised 12 June 2018; Accepted 2 July 2018; Published 10 September 2018

Academic Editor: Paulo Fonseca



We report experimental observations of permeation of $CO_2$-rich aqueous fluids of varied acidic potential (pH) on three different shales to investigate mechanical, chemical, and mineralogical effects on fracture permeability evolution. Surface profilometry and SEM-EDS (scanning electron microscopy with energy-dispersive X-ray spectroscopy) methods are employed to quantify the evolution in both roughness on and chemical constituents within the fracture surface. Results indicate that, after 12 hours of fluid flow, fracture effective hydraulic apertures evolve distinctly under different combinations of shale mineralogy, effective stress, and fluid acidity. The evolution of roughness and transformation of chemical elements on the fracture surface are in accordance with the evolution of permeability. The experimental observations imply that (1) $CO_2$-rich aqueous fluids have significant impact on the evolution of fracture permeability and may influence (and increase) shale gas production; (2) shale mineralogy, especially calcite mineral, decides the chemical reaction and permeability increasing when $CO_2$-rich aqueous fluids flow through fractures by free-face dissolution effect; (3) clay mineral swelling reduces fracture aperture and additively calcite pressure solution removes the bridging asperities, which are the main reasons for fracture permeability decrease; (4) competition roles among clay mineral swelling, mineral pressure solution, and free-face dissolution determine how fracture permeability changes. Furthermore, a multiple parameter model is built to analyze effective hydraulic aperture evolution in considering above three mechanisms, which provide a reference to forecast fracture permeability evolution in shale formations.

## 1. Introduction

Researches verified that supercritical carbon dioxide (Sc-$CO_2$) may work as fracturing fluid in shale stimulation works, which could create fractures surface with higher roughness and form complex fracture networks [1–4]. As the main channels for gas and oil transport, fracturing-induced fracture characteristics directly affect gas or oil production [5]. However, fracturing operations have a long-term component, featuring fluid-rock interaction. After fractures and channels are created, these fractures become the main conduits for fluid flow, such as fracturing fluid, methane, and oil. When using Sc-$CO_2$ fracturing stimulation, the remnant $CO_2$ reacts with native water in the shale to create $CO_2$-rich aqueous fluids, which may impact long-term permeability evolution in the reservoir.

The permeability evolution of fractures is controlled by various factors including fracture surface mineral composition [6, 7], fluid characteristics [8, 9], effective stress [10–12], and advective-diffusive transport of dissolved minerals [13, 14]. Permeability may increase due to free-face dissolution and chemical reaction by etching the fracture voids due to chemical dissolution [15] while permeability decrease could result from fracture asperity bridging by pressure solution [16, 17], stress corrosion cracking-induced diffusion [18], clay mineral swelling, and secondary mineral precipitation [19, 20]. Those opposite phenomena, which always evolve concurrently, have been observed not only in experiments but also in engineering works [21, 22]. Among the controlling factors, the role of mechanical and nonequilibrium chemical effects on fracture permeability evolution is

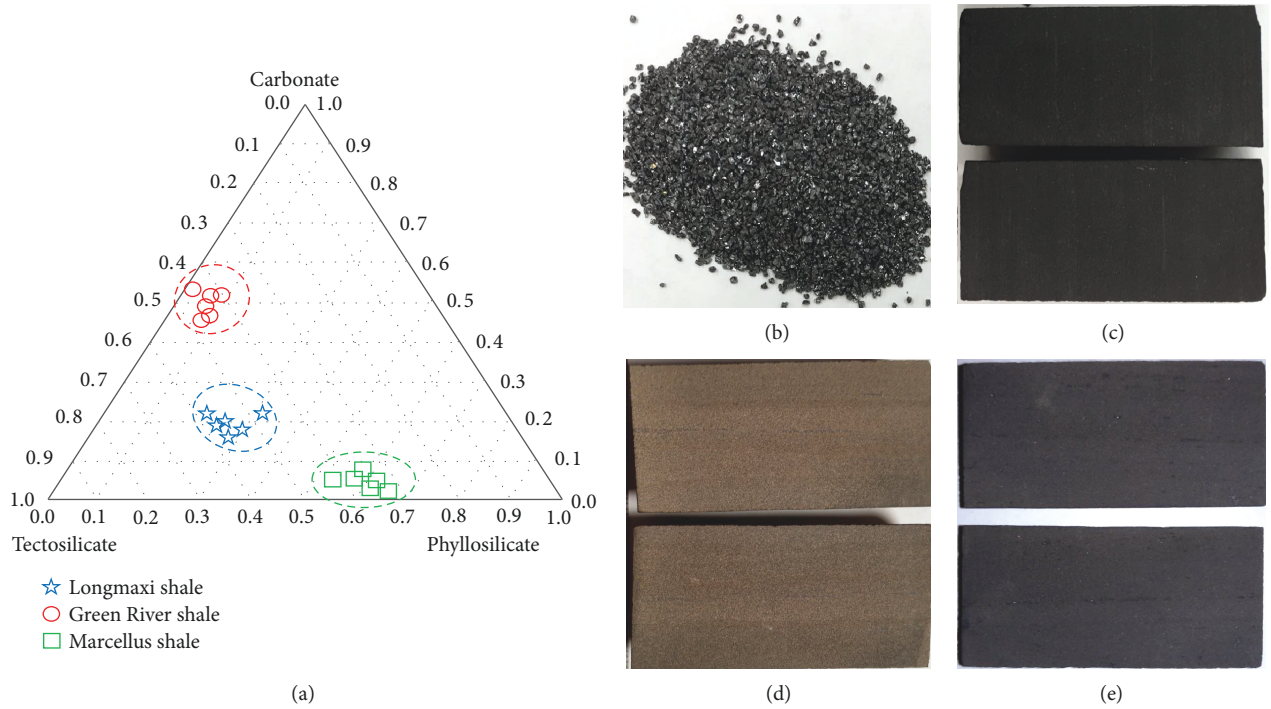


Figure 1: (a) Mineralogical composition of shale samples used in experiment, (b) 20 grit silicon carbide, (c) Longmaxi shale, (d) Green River shale, and (e) Marcellus shale.

clear [23]. However, to date, a conclusive view of permeability evolution in fracture has not evolved to define response a priori for arbitrary effective stress, mineralogy, and reactive chemistry of the fluid especially whether fracture permeability will reinforce or cancel considering mineralogical, mechanical, and chemical effects in shale where kinds of minerals exist.

Thus, the key purpose of this research is to investigate the factors that control the evolution of fracture permeability in shale when $CO_2$-rich aqueous fluids flow through. Experiments are conducted under various effective stresses and fluids with variable acidity for three kinds of shale. Measurements of the evolution of fracture permeability are combined with fracture surface profilometry and SEM-EDS (scanning electron microscopy with energy-dispersive X-ray spectroscopy) imaging to characterize fracture surface roughness evaluation and monitor changes in chemical elemental composition. Based on experimental observation and theoretical analysis, a multiple parameter model is developed to forecast the permeability evolution in shale which considers mineral pressure solution, free-face dissolution, and clay mineral swelling.

## 2. Experimental Process

Experimental study consists of three interrelated components: (1) core flooding experiments with different confining pressure (3.0 MPa, 5.0 MPa, and 10.0 MPa) and fluid acidity (pH = 4.0, 5.0, 6.0, and 7.0) in Longmaxi, Green River, and Marcellus shales; (2) microcharacterization of fracture surfaces to define fracture surface roughness evolution; and (3) measurement of the change in chemical constituents on the fracture surface by chemical reaction.

*2.1. Sample Materials and Preparation.* Three natural shales with different minerology—Longmaxi shale, Green River shale, and Marcellus shale—are selected. Longmaxi shale is a fine-grained black shale, highly laminated with low-grade kerogen [19], which is a principal shale gas producer in Chongqing, China. Green River shale is recovered from a freshwater lacustrine environment in Grand Junction, Colorado, and Marcellus shale is extracted from outcrop from Middle Devonian Marcellus Formation at Frankstown, Pennsylvania (40°26′00″ N, 78°20′28″ W). The mineral composition of the above three shales was determined by powder X-ray diffraction (XRD) analysis, and results are shown in Figure 1(a).

Core flooding experiments were conducted on cylindrical cores (25.4 mm in diameter and 50.8 mm in length). Previous experiments indicated that Sc-$CO_2$ fracturing creates unparalleled fracture surfaces which are not suitable for core flooding tests [1]. Hence, rock sample was firstly saw-cut into two halves with smooth fracture surface and then uniformly roughened with various abrasive silicon carbides (10, 20, 30, and 60 grits) to yield a controlled fracture topography. Profilometry tests quantitatively validate that 20 grit-polished surfaces have similar surface roughness characteristics and effectively analogue the fracture surfaces induced by Sc-$CO_2$ fracturing (Table 1). The samples used in experiments are shown in Figures 1(c)–1(e).

In Table 2, $S_a$ is the arithmetic mean of the absolute value of the height expressed as $S_a = 1/A \int |z(x, y)| dxdy$; $S_q$ is the root mean square (RMS) of ordinate values within

Table 1: Detailed mineralogical compositions (wt%) of each samples.

| Mineral category | Mineral name | Longmaxi shale | | Green River shale | | Marcellus shale | |
|---|---|---|---|---|---|---|---|
| Tectosilicate | Quartz | 51.6 | 55.3 | 14.9 | 45.9 | 36.1 | 36.1 |
| | Analcime | 0 | | 16.7 | | 0 | |
| | Anorthite | 0 | | 7.8 | | 0 | |
| | Albite | 3.7 | | 0 | | 0 | |
| | Microcline | 0 | | 6.5 | | 0 | |
| Carbonate | Dolomite | 3.4 | 20.1 | 39.4 | 51.8 | 0 | 0 |
| | Calcite | 16.7 | | 12.4 | | 0 | |
| Phyllosilicate | Muscovite | 0 | 24.6 | 0 | 2.3 | 10.4 | 63.9 |
| | Illite | 24.6 | | 2.3 | | 37.4 | |
| | Chlorite | 0 | | 0 | | 0 | |
| | Kaolinite | 0 | | 0 | | 4.9 | |
| | Montmorillonite | 0 | | 0 | | 11.2 | |
| Total | | 100 | 100 | 100 | 100 | 100 | 100 |

Table 2: Comparison of topography between artificial samples and Sc-$CO_2$-fractured samples.

| Sample description | $S_a$ ($\mu$m) | $S_q$ ($\mu$m) |
|---|---|---|
| Sc-$CO_2$ fractured | 18.32 | 23.03 |
| 10 grit silicon carbide polished | 21.39 | 26.88 |
| 20 grit silicon carbide polished | 18.44 | 23.99 |
| 30 grit silicon carbide polished | 17.99 | 21.77 |
| 60 grit silicon carbide polished | 15.22 | 19.34 |

the definition area and defined as $S_q = 1/A^2 \int |z^2(x, y)| dxdy$. $A$ is the scan area.

*2.2. Preparation of Carbonic Acid.* At room temperature (25°C) and atmospheric pressure ($1.013 \times 10^5$ Pa), the lowest pH of $CO_2$-rich distilled water is about 3.92 [8]. Hence, we inject $CO_2$ gas into distilled water to generate $CO_2$-rich aqueous fluids with different fluid acidity at room temperature. The pH of the fluid is controlled according to the following reactions:

$$\begin{aligned} H_2CO_3 &\rightleftharpoons HCO_3^- + H^+ \\ HCO_3^- &\rightleftharpoons CO_3^{2-} + H^+ \end{aligned} \quad (1)$$

The prepared fluid is immediately injected into the pump to retain the $CO_2$ dissolved in the distilled water and to maintain a constant fluid acidity.

*2.3. Experimental Configuration and Procedure.* A standard triaxial apparatus for the core flooding experiment is shown in Figure 2. The flow rate of the pump was recorded. For convenience of calculation, effective hydraulic aperture is used to evaluate fracture permeability due to the fluid flow in this setup is laminar flow. The effective hydraulic aperture of the fracture is calculated through the cubic law as

$$e_h = \left( -\frac{12\mu LQ}{W\Delta P} \right)^{1/3}. \quad (2)$$

In this equation, $e_h$ (m) is the effective hydraulic aperture; $Q$ ($m^3$/s) is the recorded flowrate; $\Delta P$ (Pa) is the differential pressure; $\mu$ (Pa·s) is the viscosity of the injected fluid; $L$ (m) and $W$ (m) are the lengths of the fracture in the directions parallel and perpendicular to the flow direction.

*2.4. Optical Profilometry Analysis.* Optical profilometry was performed both before and after the core flooding experiments using a Zygo™ NewView optical profilometer (Figure 3(a)) to quantify the roughness change on shale fracture surface. Surface roughness is a quantified RMS as noted previously.

Before the core flooding experiment, a Teflon film mask was carefully attached to each fracture surface with observation windows along flow direction (Figure 3(c)). Three windows were picked along the central line, parallel to the flow direction. The Teflon film was taken off when the sample was installed into the flow cell. At the completion of each core flooding experiment, the sample would be removed and opened into two halves, and Teflon would be placed back again, aligned, and the profilometry measurements repeated immediately after each core flooding experiment. This enables a same area is scanned before and after core flooding tests, and wet conditions of samples also avoid clay dehydration and induced potential roughness change.

*2.5. SEM-EDS Analysis.* We also scan these three windows using SEM-EDS (scanning electron microscopy with X-ray microanalysis) which quantitatively analyze the change in chemical constituents on the fracture surface before and after the core flooding experiments. The scanning apparatus is FEI Quanta 600 (Figure 3(b)). In this analysis, we investigate the role of fluid acidity on fracture surface chemical element changes.

## 3. Experiment Results

In this part, we present the core flooding experiment results for three different kinds of shale—Longmaxi shale,

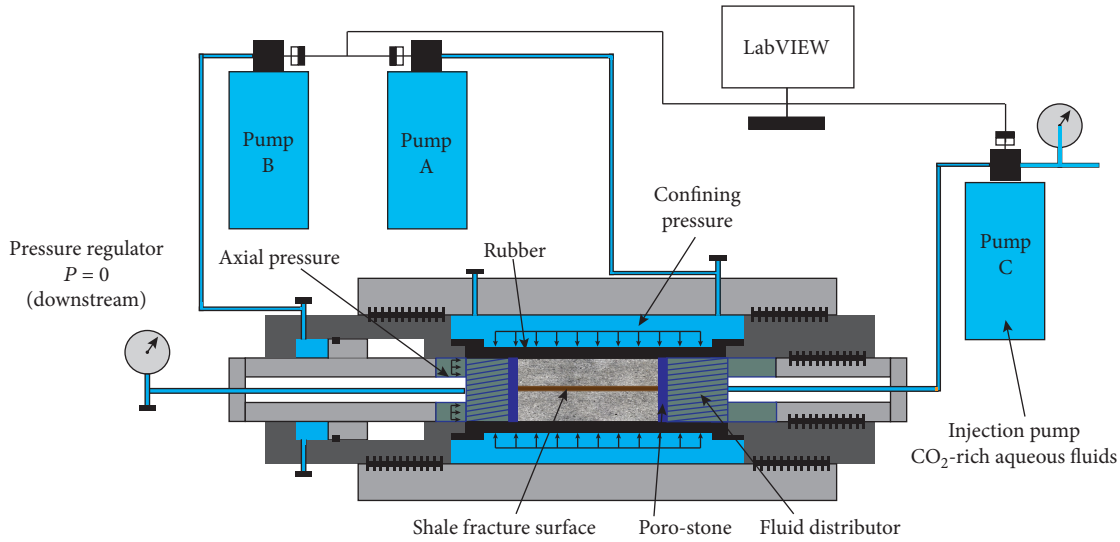


Figure 2: Experimental configuration for core flooding experiments: pump A controls the confining pressure (normal stress) applied on the fracture. Pump B controls axial pressure which is set to 500 kPa to ensure that the piston contacts with tightly with the sample. Pump C injects fluid with a different acidity at a constant pressure of 120 kPa. The prepared sample is placed between two stainless steel end platens faced with flow distributors and sealed within a latex membrane.

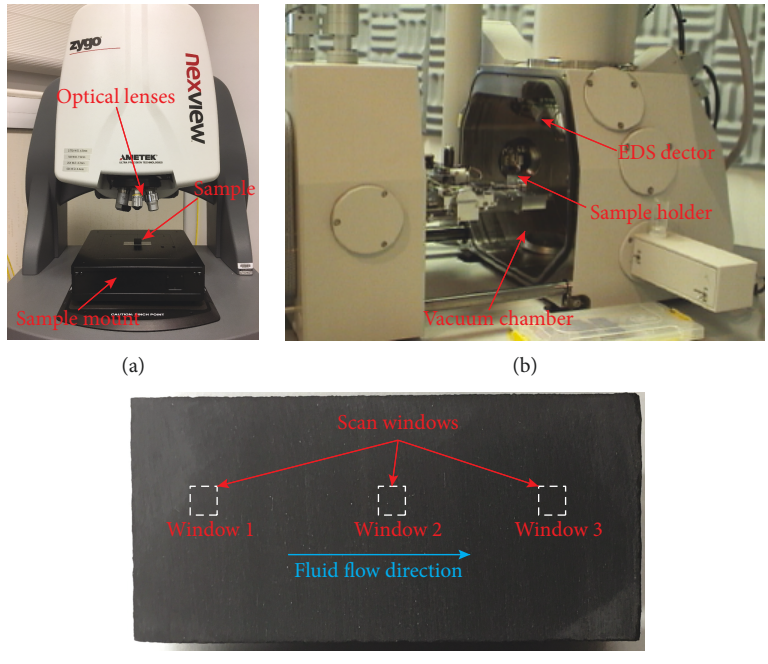


Figure 3: (a) Optical profilometry used in experiment, (b) SEM apparatus used in experiments, and (c) profilometry and SEM scan area before and after core flooding tests. The dimension of each window is 1.8 mm × 1.8 mm.

Green River shale, and Marcellus shale—and discuss the experimental observations. Additionally, profilometry results are summarized for the single condition of 10 MPa confining stress but various fluid acidities. Finally, chemical element changes are shown within the fracture surfaces under 10 MPa confining stress and various fluid acidities by SEM-EDS analysis.

*3.1. Effective Stress Control on Permeability Evolution for Longmaxi Shale.* The evolution of effective hydraulic aperture under different effective stresses (3.0, 5.0, and 10.0 MPa) and fluid acidity (fluid pH equals to 4.0, 5.0, 6.0, and 7.0) is shown in Figure 4 for Longmaxi shale. The curves have a similar trend when fluid acidity is the same while confining stress changes. Thus, confining stress plays a minor role

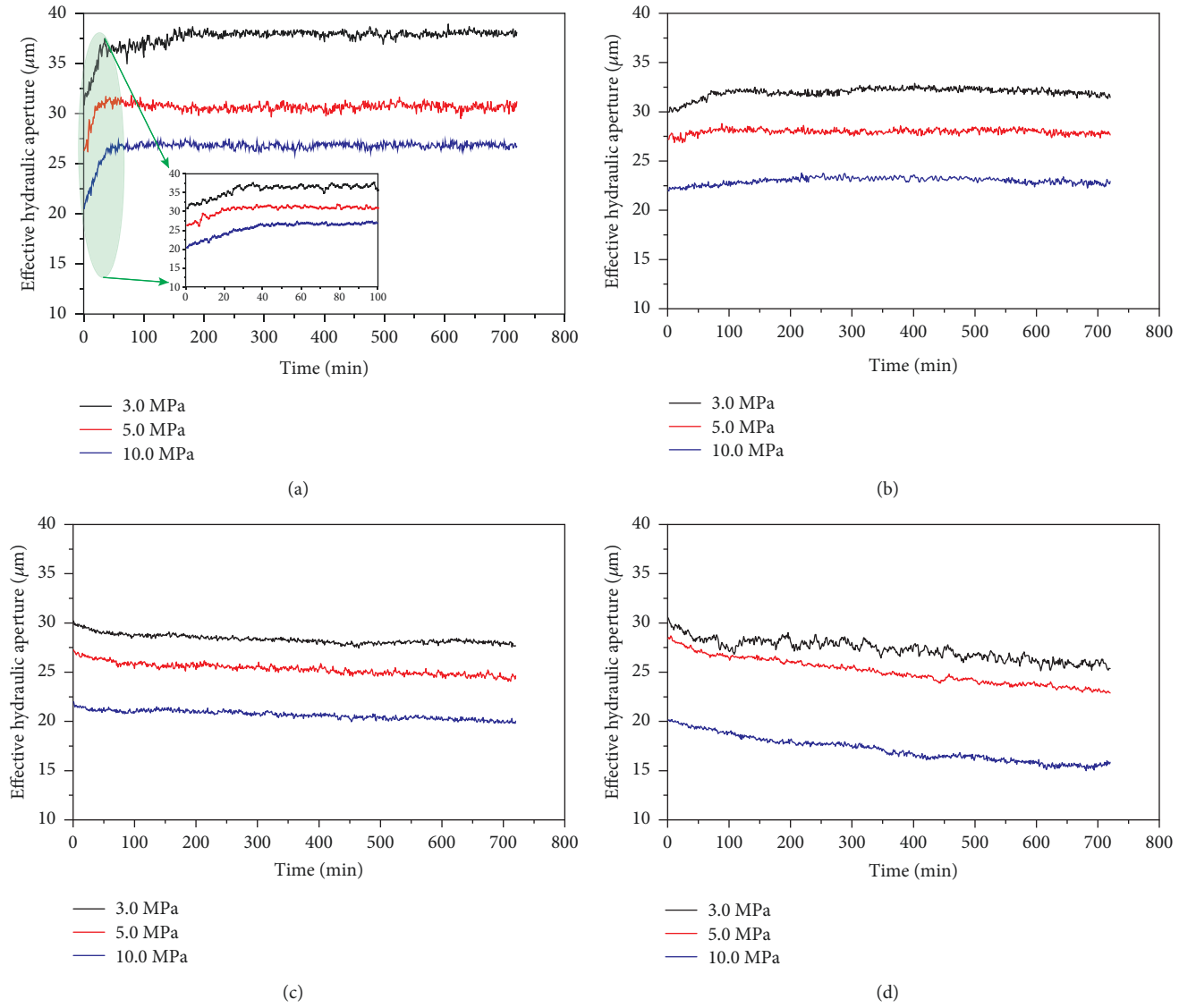


Figure 4: Effective hydraulic aperture evolution with time under different confining stresses for Longmaxi shale. (a) Fluid pH = 4.0 condition and the subplot is an expanded figure during the period of effective hydraulic aperture increase, (b) fluid pH = 5.0, (c) fluid pH = 6.0, and (d) fluid pH = 7.0. A monotonic increase in effective hydraulic aperture until a maximum aperture is observed for fluid pH = 4.0 and 5.0 condition. Following this, the fracture aperture has a relatively small change. Sustained decrease of effective hydraulic aperture is observed during the 12-hour core flooding experiments when fluid pH = 6.0 and 7.0.

in controlling fracture effective hydraulic aperture evolution. In addition, confining stress controls the initial aperture and initial flow rate since a stable pressure difference is applied between upstream and downstream reservoirs.

*3.2. Mineralogical Control on Permeability Evolution.* Figure 5 indicates the vital influence of mineralogical control on permeability evolution. Even the fluid acidity is the same, permeability evolves differently for shale with various mineralogical compositions. Marcellus shale has a permeability decrease trend under all combinations of fluid acidity and confining stress. For Longmaxi shale and Green River shale, permeability increases when fluid pH equals to 4.0 and 5.0 while decrease when fluid pH equals to 6.0 and 7.0. Hence, when predicting fracture permeability evolution, the mineralogical compositions of shale should be taken into consideration.

*3.3. Fluid Acidity Control on Permeability Evolution.* As shown in Figure 6, fluid acidity has a dominant effect on effective hydraulic aperture change for all three kinds of shale. For Longmaxi shale and Green River shale, an effective hydraulic aperture increase could be observed in first few hours before a maximum value is reached when fluid pH = 4.0 and 5.0. While injected fluid pH = 6.0 and 7.0, a monotonic decrease is observed for both Longmaxi shale and Green River shale, and larger decrease trend is observed for fluid pH = 7.0 condition. For Marcellus shale, the effective hydraulic aperture keeps constantly decrease while larger decrease trend is observed when fluid acidity is low.

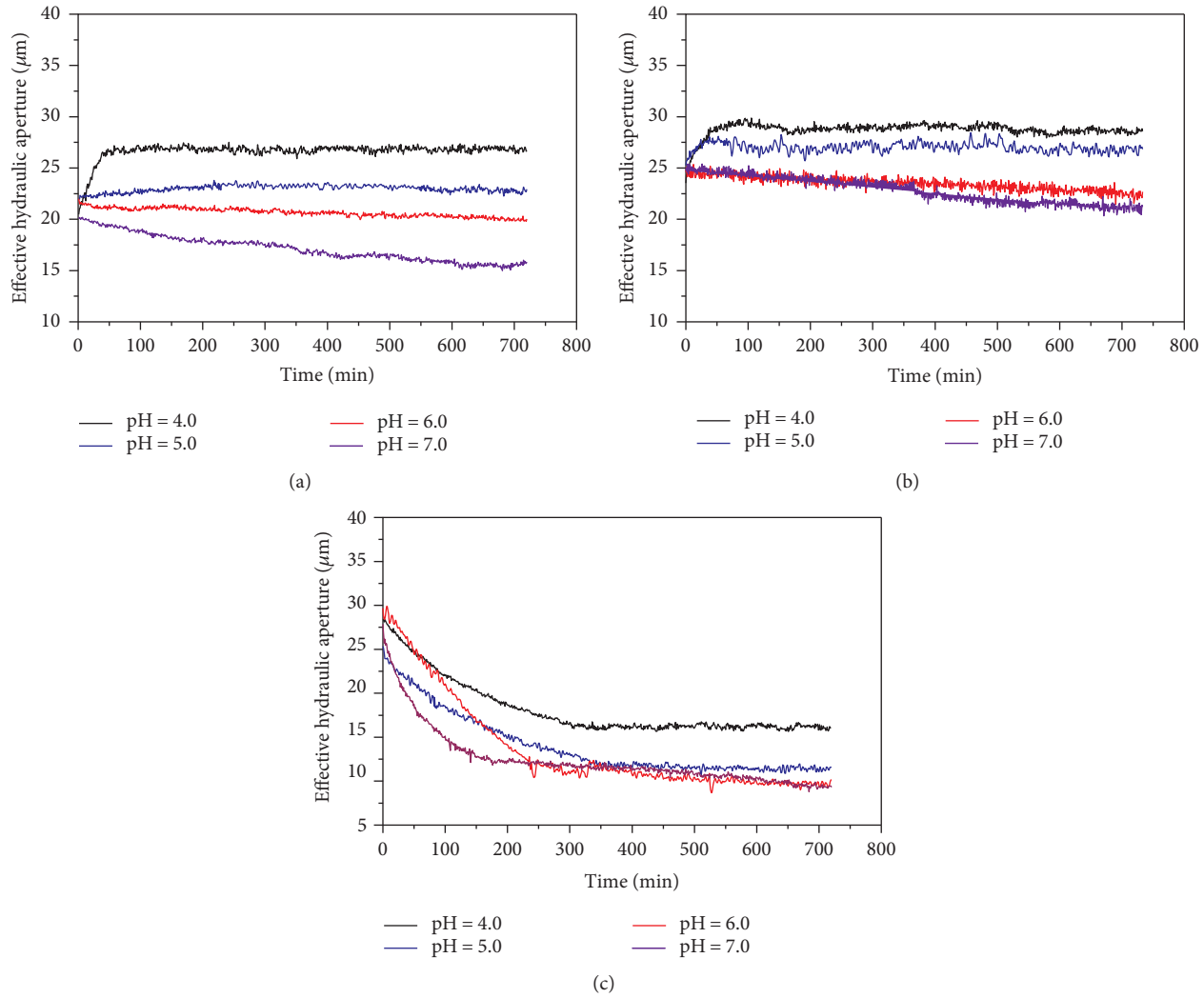


Figure 5: Effective hydraulic aperture evolution with time under different fluid acidity conditions for various shales. (a) Longmaxi shale, (b) Green River shale, and (c) Marcellus shale. When fluid pH = 4.0 and 5.0, there is a monotonic increase in effective hydraulic aperture until a maximum aperture is observed for Longmaxi shale and Green River shale. The effective hydraulic aperture keeps a decrease trend for Longmaxi shale and Green River shale when pH = 6.0 and 7.0 while all fluid acidity conditions for Marcellus shale.

*3.4. Summary of Permeability Evolution.* Total fracture permeability change after core flooding tests is summarized in Figure 7, which indicates fluid acidity has a significant effect on fracture permeability evolution in shale. Fracture permeability increases one time for Longmaxi shale and Green River shale when high acidity fluid flow through, while fracture almost decreases half for Marcellus under various pH fluid conditions. This is an implication for shale gas production, where after Sc-$CO_2$ fracturing, single fracture permeability may increase largely and benefits to shale gas recovery.

*3.5. Fracture Surface Roughness Evolution.* The evolution of fracture surface roughness contributes to the evolution of fracture aperture with different fluid acidity. Relationship between roughness change and permeability evolution is cleared in Figure 8.

When RMS roughness increases, it means more peaks and valleys are created in fracture surface, which increases the porosity and more channels are formed for fluid flow within fracture and increase fracture permeability. In contrast, when fracture roughness decreases, since a normal confining stress is applied, mineral particles in peak areas are dissolved and precipitated in noncontacting areas, which makes peaks and valleys disappear in fracture surface, thus decrease the porosity and fracture permeability.

In Figure 9, we show changes of parameters ΔRMS both before and after fluid flow in masked windows 1, 2, and 3 under different fluid acidity conditions for different shale (confining stress equals to 10.0 MPa). In this plot,

$$\Delta\mathrm{RMS} = \mathrm{RMS}_{(\mathrm{after})} - \mathrm{RMS}_{(\mathrm{before})}. \quad (3)$$

A similar roughness evolution trend is observed for Longmaxi shale and Green River shale while Marcellus shale has a distinct behavior.

After core flooding tests, Marcellus shale fracture roughness is always smaller than that before tests for all three

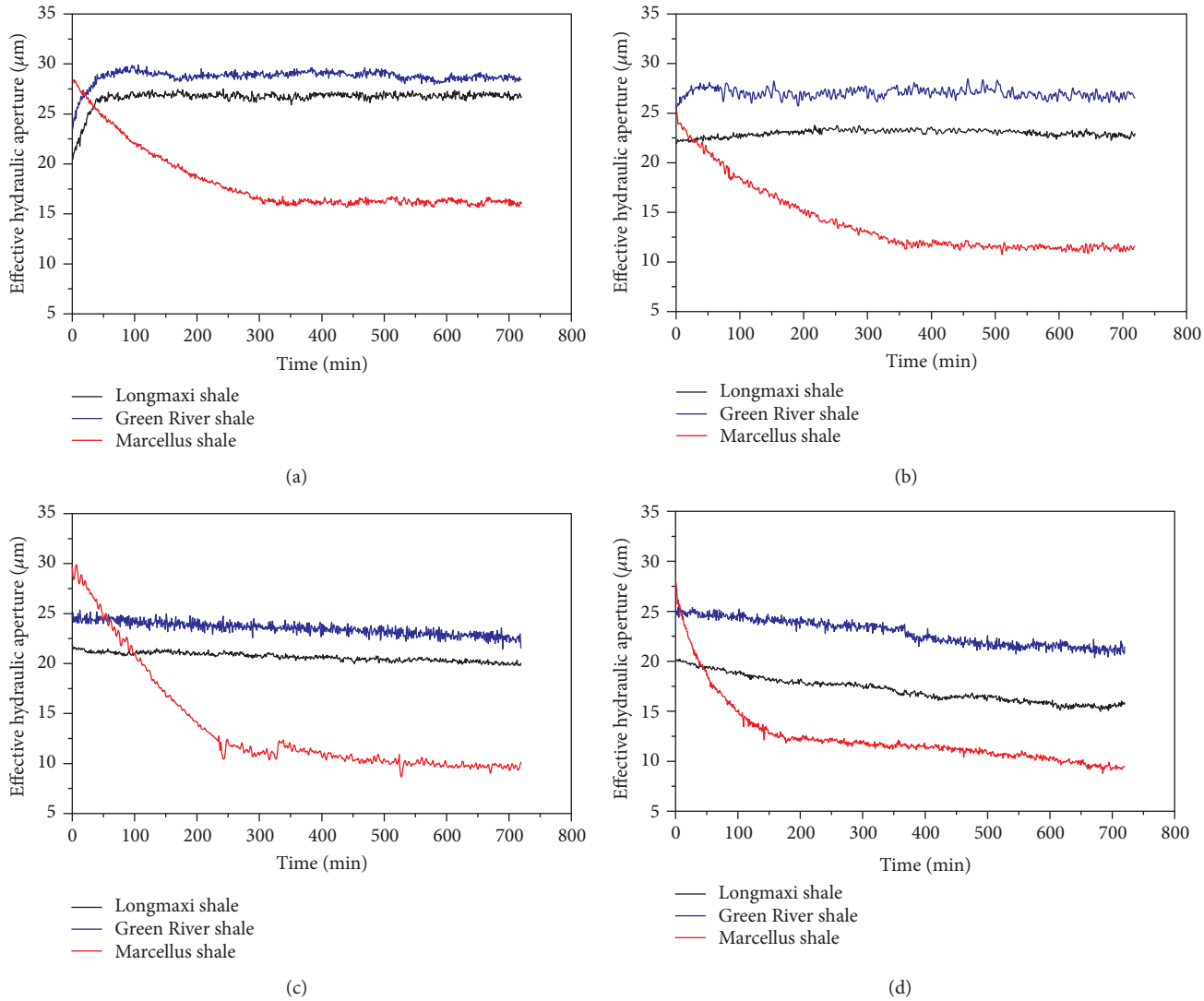


Figure 6: Aperture evolutions with time for various shale. (a) Fluid pH = 4.0, (b) fluid pH = 5.0, (c) fluid pH = 6.0, and (d) fluid pH = 7.0. For shale with different mineralogical composition, aperture evolution shows distinct trend. Higher acidic fluid increases the aperture for Longmaxi shale and Green River shale while lower acidic fluid close fractures for all three kinds of shale.

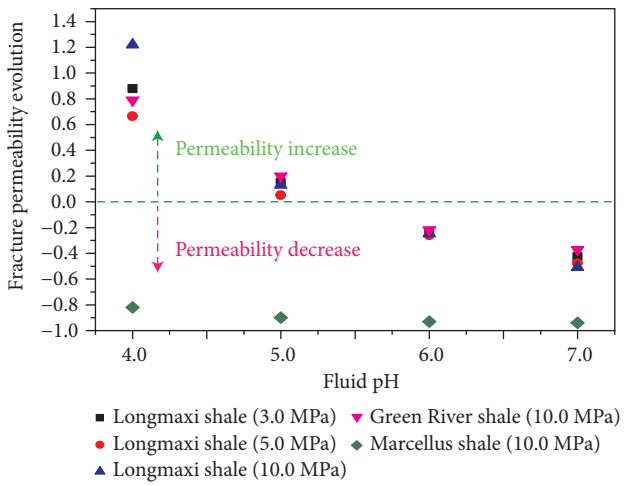


Figure 7: The summary of fracture permeability evolution results.

windows. This observation is in accordance with permeability decreasing. The reason could be the clay swelling since there is no calcite mineral in Marcellus shale, where mineral pressure solution and free-face dissolution are really weak. As shown in Table 1, the main clay mineral in Marcellus shale is illite (37.4%) and montmorillonite (11.2%). Montmorillonite mineral is regarded as swelling clay for the reason that water molecules easily enter the interlayer along the silicon-oxygen plane, which will increase the distance between the layers and causing the volume expansion. Even though the crystal structure of illite is as same as that of the montmorillonite minerals, $K^+$ ion is embedded in the hexagonal cavity of the clay silicon oxide layers and decreases the hydration capacity, which leads to weakly volume expansion. Hence, in this case, clay mineral swelling, specifically speaking, montmorillonite minerals swelling decreases fracture roughness, porosity, and effective hydraulic aperture. The roughness changes complicatedly for Longmaxi shale and Green River shale when injected fluid acidity varies. When the fluid

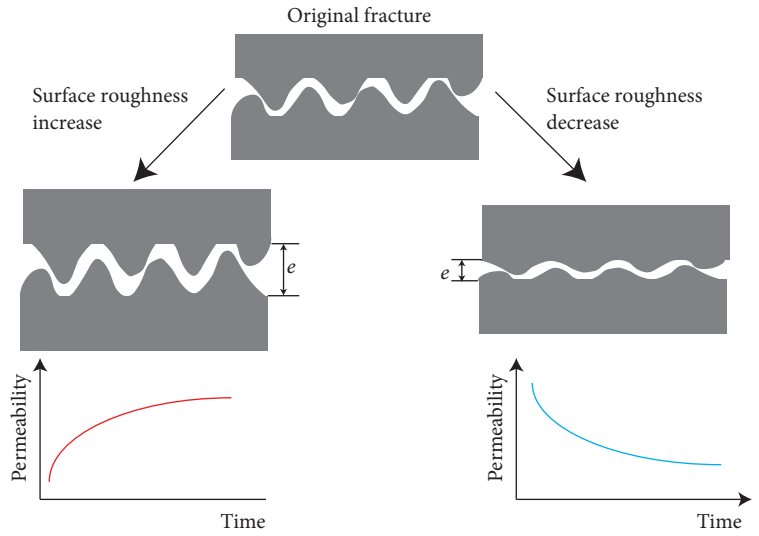


Figure 8: Schematic map of relationship between fracture roughness and permeability evolution.

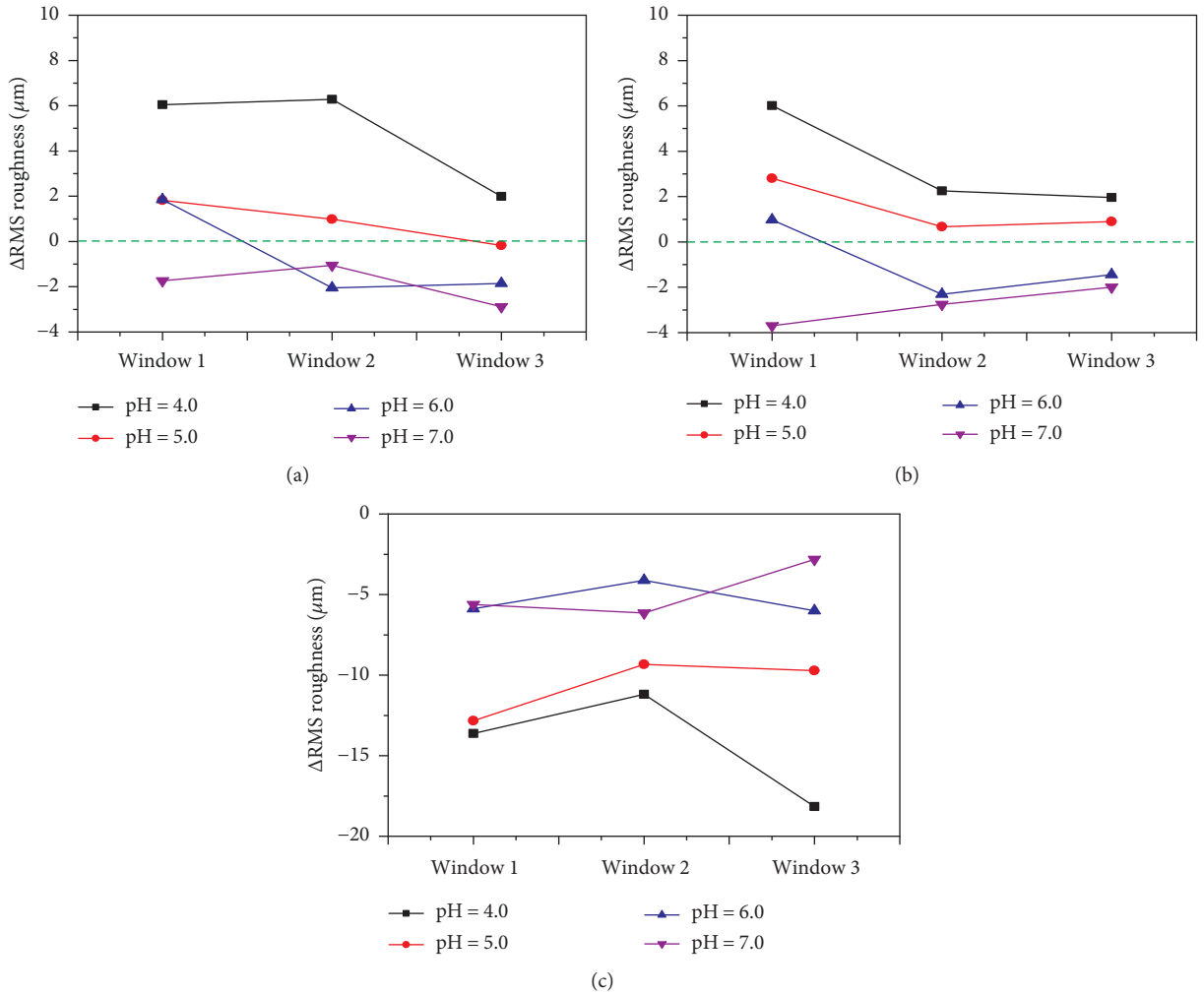


Figure 9: RMS roughness change after core flooding experiments. $x$-axis is the measurement window with fluid flow direction from left (upstream) to right (downstream). (a) Longmaxi shale, (b) Green River shale, and (c) Marcellus shale. ΔRMS larger than 0 means roughness increase and potentially fracture aperture gaping while ΔRMS smaller than 0 indicates a roughness decrease and a fracture aperture closing.

pH is 4.0, Longmaxi shale and Green River shale show an increase of roughness which contributes to fracture aperture gaping which is consistent with fracture aperture evolution trend in core flooding tests. Additionally, a similar increase value is observed at three windows even though a slight larger increase at inlet (windows 1 and 2) rather than outlet (window 3). This phenomenon is reasonable when acidic fluid flows through a fracture; acidic fluid removes calcite from upstream and equilibrates the fluid—staunching any downstream dissolution. Besides, hydraulic effect that some mineral particles may be removed in inlet area and precipitate in outlet area also contributes to the less roughness increase in the outlet area. The reason is that precipitation of minerals mainly happens in the noncontacting areas since there is no space for minerals to precipitate in the contacting areas. The precipitations in the noncontacting areas, which we regard as valleys in fracture surface, the precipitated minerals fill the voids and valleys, which decrease the fracture roughness. In addition, the minerals mainly come from the contacting areas caused by pressure solution effect, which also dissolve the peaks in fracture surface. The height decrease of peaks and height increase in valleys both contribute to the roughness decrease.

When the fluid pH = 5.0, a similar trend is apparent to that at fluid pH = 4.0 for Longmaxi shale and Green River shale. However, the impact of chemical reaction on roughness is smaller than at fluid pH = 4.0, due to the lower reactivity between acidic fluid and calcite.

When the fluid pH = 6.0, window 1 shows a relatively small increase in roughness for both Longmaxi shale and Green River shale. This means that the fluid has little reaction with calcite while at windows 2 and 3 both show a roughness decrease due to mineral pressure solution and clay swelling. Hence, the pH = 6.0 fluid is not sufficiently reactive to open the fracture by reactive dissolution while mineral pressure solution dominates aperture evolution and in fracture closing and the destruction of permeability.

When the fluid pH = 7.0, all three windows show a decrease in roughness, which contributes to the fracture aperture closing. Minerals dissolve and redistribute over the fracture surfaces. Initial peaks and valleys in the fracture surface are filled with dissolved minerals and result in a decrease in the roughness and finally a closing of the fracture aperture.

### 3.6. Surface Structure and Chemical Transformations

*3.6.1. Surface Structure Change after Core Flooding Tests.* As shown in Figure 10, the acidic fluid changes the surface structure after core flooding tests. The fracture surface structure is complete, and minerals are almost well distributed before tests for all three kinds of shale. However, after acidic fluid flow through, the fracture surface structure changes differently.

For Longmaxi shale and Green River shale, surface structure changes dramatically. When fluid pH = 4.0, many voids and large pores are observed. With a decrease in fluid acidity, fewer voids are apparent in the SEM images. Compared with the corresponding EDS images, Ca element disappears after core flooding tests when fluid pH equals to 4.0 and 5.0. We believe the large voids and pores result from calcite removal. However, for Marcellus shale where no calcite mineral exists, the fracture surface structure keeps stable and no large pores are observed. Hence, we assure that the calcite mineral plays a vital role in determining fracture surface structure evolution by reaction with acidic fluid.

*3.6.2. Chemical Transformations after Core Flooding Tests.* The percent change in Ca abundance is plotted in Figure 11. To investigate the change in mass, ΔCa represents the weight percentage change as

$$\Delta\mathrm{Ca} = \frac{n_{\mathrm{Ca(after)}} - n_{\mathrm{Ca(before)}}}{n_{\mathrm{Ca(before)}}}. \quad (4)$$

In this equation, $n_{\mathrm{Ca(before)}}$ and $n_{\mathrm{Ca(after)}}$ are the weight percentages of Ca element both before and after the core flooding tests.

In Figure 11, when the inlet fluid pH = 7.0, the 20% Ca element removal may be the reason for mineral pressure solution of fracture asperities and which causes calcite to be dissolved in Longmaxi shale. Those removed calcite particles flow out with fluid and cause the percentage decrease of Ca element, which attributes to the calcite having larger solubility and dissolution rate in water than quartz and any other minerals in the Longmaxi shale; when the inlet fluid pH = 4.0, 5.0, and 6.0, the Ca concentration decreases significantly compared with for the flow of distilled water. When the fluid pH = 4.0 and 5.0, more than 80 percent of the Ca is removed from the fracture surface.

Trend is similar while value is different for Green River shale. Less Ca element disappeared from fracture surface attributes to the dolomite minerals ($CaMg(CO_3)_2$). Unlike calcite ($CaCO_3$) which has chemical reaction with acid fluid and dissolves in fluid, dolomite is much more stable and the Ca element in it keeps in fracture surface after core flooding tests. This phenomenon could also be observed in EDS images. Hence, Ca element still exists in Green River shale fracture surface as the mode of dolomite.

## 4. Analysis by a Multiple Parameter Model

Fracture effective hydraulic aperture evolution in shale fractures is evaluated for various combinations of confining stress (3.0, 5.0, and 10.0 MPa) and inlet fluid acidity (fluid pH = 4.0, 5.0, 6.0, and 7.0) with shale with various mineralogy (Longmaxi shale, Green River shale, and Marcellus shale). Experimental results suggest the following: (1) effective stress controls initial fracture permeability and has little effect on permeability evolution; (2) high acidic $CO_2$-rich aqueous fluids (fluid pH = 4.0 and 5.0) lead to a linear effective hydraulic fracture aperture increase for a period of time for shales with calcite while low acidic $CO_2$-rich aqueous fluid makes fracture close; (3) for shale with high clay content, the fracture permeability keeps decreasing with a gradually smaller decrease rate. In this part, we discuss the fracture aperture evolution quantitatively by a multiple parameter model which considers mineral pressure solution, free-face dissolution, and clay swelling effects.

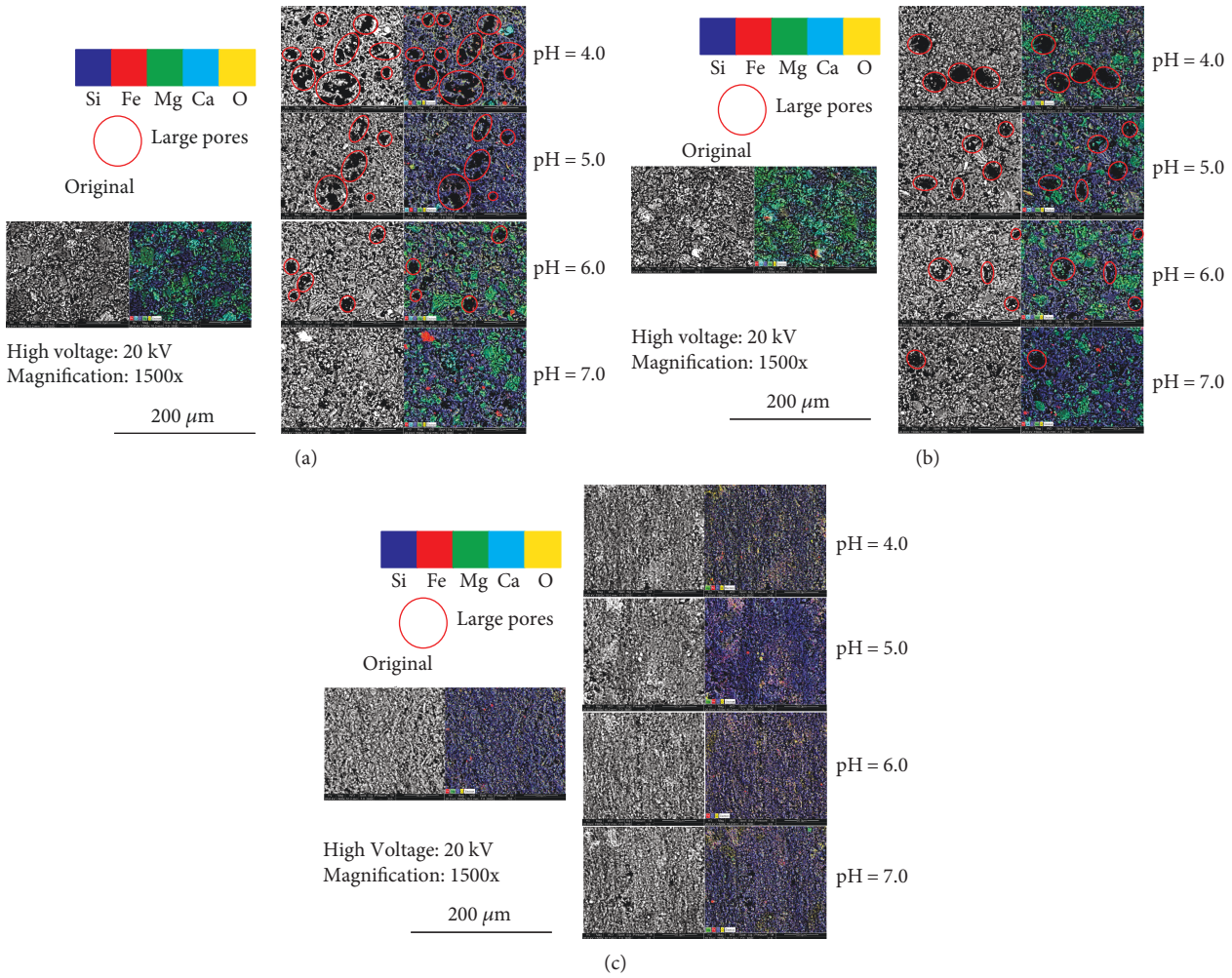


Figure 10: SEM images and corresponding EDS images of the fracture surface (window 1) after core flooding tests under various fluid pH when confining stress is 10 MPa. (a) Longmaxi shale, (b) Green River shale, and (c) Marcellus shale.

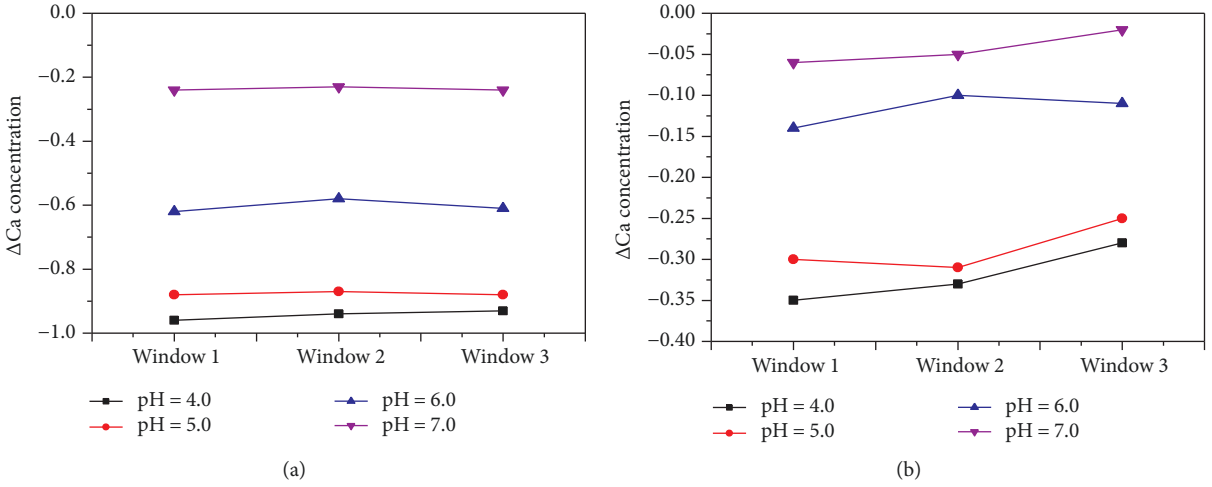


Figure 11: Ca concentration change after the core flooding experiment. (a) Longmaxi shale and (b) Green River shale.

*4.1. Effective Hydraulic Aperture Decrease Due to Pressure Solution.* As shown in Figure 12(a), pressure solution leads to aperture closing which happens at contacting asperities. The minerals in contacting asperity dissolve in flowing fluid due to the high contact force, and the dissolution minerals transport along an interfacial water film to the fracture void

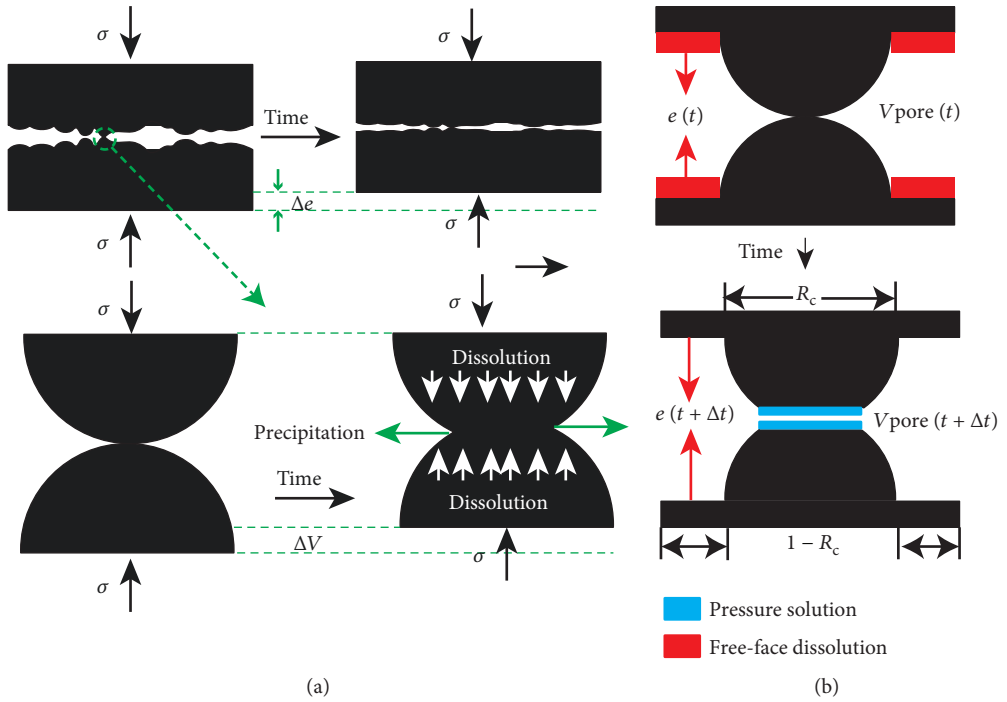


Figure 12: Schematic illustration of pressure solution in contacting asperities and free-face dissolution in noncontacting areas. (a) Pressure solution occurs in contacting asperities and decreases the fracture aperture and (b) mineral dissolution at the free face contributes to the fracture aperture increase.

which makes mineral redistributes within the fracture void by precipitation.

The contacting asperities are simplified as spherical contact, and the mineral mass precipitated into fracture voids comes from the dissolution as the asperity contacts are expressed as [24]

$$\frac{dM_{\text{diss}}^{\text{ps}}}{dt} = \frac{3\pi V_{\text{m}}^2(\sigma_{\text{a}} - \sigma_{\text{c}})k_1\rho_{\text{g}}d_{\text{c}}^2}{4RT}. \quad (5)$$

In this equation, $dM_{\text{diss}}^{\text{ps}}/dt$ is the dissolution mass flux caused by pressure solution; $V_{\text{m}}$ is the molar volume of solid ($3.69 \times 10^{-5}$ mol$^{-1}$ for calcite, $2.27 \times 10^{-5}$ mol$^{-1}$ for quartz); $\sigma_{\text{c}}$ is the critical stress; $\sigma_{\text{a}}$ is the stress acting on grain-to-grain contacts exceeds the hydrostatic pore pressure, and when $\sigma_{\text{a}} = \sigma_{\text{c}}$, the system will be an equilibrium state that the pressure in contacting asperities is equal to critical stress and pressure solution phenomenon is terminated; $R$ and $T$ are gas constant and temperature, respectively; $k_1$ is the dissolution rate constant of mineral; $\rho_{\text{g}}$ is the density of solid; $d_{\text{c}}$ is the contact diameter of asperity; $\sigma_{\text{c}}$ could be expressed as [25]

$$\sigma_{\text{c}} = \frac{E_{\text{m}}(1 - (T/T_{\text{m}}))}{4V_{\text{m}}}, \quad (6)$$

where $E_{\text{m}}$ and $T_{\text{m}}$ are heat and temperature of fusion. Since the critical stress is largely affected by temperature. At room temperature (25°C), the $\sigma_{\text{c}} = 198.56$ MPa for calcite and 8520 MPa for quartz. However, the calculated critical stress (198.56 MPa) for calcite is modified so that a large decrease in effective hydraulic aperture (8 mm) can be predicted [24]. Hence, in this model, the modified critical stress (20 MPa) for calcite will be used for later calculation.

*4.2. Effective Hydraulic Aperture Increase Due to Free-Face Dissolution.* Imbalance of the solute concentration makes mineral dissolves and precipitates from the fracture surface in noncontacting areas, which is the chemical effect on fracture aperture gaping [26].

As shown in Figure 12(b), the mineral dissolution rate at noncontacting areas (free-face dissolution) is expressed as [10, 21]

$$\frac{dM_{\text{diss}}^{\text{ff}}}{dt} = 2 \cdot k_2 \cdot A_{\text{local}} \cdot (1 - R_{\text{c}}) \cdot \rho_{\text{g}} \cdot V_{\text{m}} \cdot \left(1 - \frac{C_{\text{pore}}}{C_{\text{eq}}}\right), \quad (7)$$

where $k_2$ is the dissolution rate of minerals at the free-face area, $C_{\text{pore}}$ is the concentration of mineral in the pore space, and $C_{\text{eq}}$ is the equilibrium solubility of mineral. Since free-face dissolution happens in both halve fractures, a constant 2 is added in (4).

Pressure solution and free-face dissolution happen simultaneously to control the fracture aperture evolution. Now, as illustrated in Figure 12(b), at a specific time, $t$, the relationship between fracture aperture $e_{\text{h}}(t)$ and pore volume in a representative elemental volume $A_{\text{local}}$ could be expressed as

$$V_{\text{pore}}(t) = e_{\text{h}}(t) \cdot A_{\text{local}}. \quad (8)$$

Given a time step $\Delta t$, the pore volume will change to $V_{\text{pore}}(t+\Delta t)$ for the reason of pressure solution and free-face dissolution

$$\begin{aligned} V_{\text{pore}}(t+\Delta t) &= V_{\text{pore}}(t) - \frac{dM_{\text{diss}}^{\text{ps}}}{dt}\cdot\frac{1}{\rho_{\text{g}}} \\ &\quad\cdot\Delta t\cdot\frac{1-R_{\text{c}}}{R_{\text{c}}} + \frac{dM_{\text{diss}}^{\text{ff}}}{dt}\cdot\frac{1}{\rho_{\text{g}}}\cdot\Delta t \\ &= e_{\text{h}}(t+\Delta t)\cdot A_{\text{local}}. \end{aligned} \tag{9}$$

Hence, the fracture aperture changing rate is expressed as

$$\begin{aligned} \frac{de_{\text{h}}}{dt} &= \frac{e_{\text{h}}(t+\Delta t)-e_{\text{h}}(t)}{\Delta t} \\ &= \frac{1}{\rho_{\text{g}}\cdot A_{\text{local}}}\left(-\frac{dM_{\text{diss}}^{\text{ps}}}{dt}\cdot\frac{1-R_{\text{c}}}{R_{\text{c}}} + \frac{dM_{\text{diss}}^{\text{ff}}}{dt}\right). \end{aligned} \tag{10}$$

Equation (5) describes the dissolution mass flux caused by pressure solution and (7) describes the mineral dissolution rate at noncontacting areas (free-face dissolution), respectively. Substituting them into (10) yields

$$\begin{aligned} \frac{de_{\text{h}}}{dt} &= -\frac{3V_{\text{m}}{}^2}{RT}\cdot(1-R_{\text{c}})\left(\frac{\sigma_{\text{conf}}}{R_{\text{c}}}-\sigma_{\text{c}}\right)\cdot k_1 \\ &\quad + 2(1-R_{\text{c}})\cdot V_{\text{m}}\cdot k_2. \end{aligned} \tag{11}$$

In this equation, the first term $-(3V_m^2/RT)\cdot(1-R_{\text{c}})((\sigma_{\text{conf}}/R_{\text{c}})-\sigma_{\text{c}})\cdot k_1$ refers to the fracture aperture decrease due to pressure solution and the second term $2(1-R_{\text{c}})\cdot V_{\text{m}}\cdot k_2$ refers to the fracture aperture increase for the reason of mineral free-face dissolution.

*4.3. Effective Hydraulic Aperture Decrease Induced by Clay Swell.* Experimental and simulation works have shown that clay minerals could expand in volume up to 20 times through adsorption of water [27], which lead to fracture permeability decrease 10% to 90% based on different kinds of clay minerals and clay content in shale samples [28]. Hence, the swelling effect is considered when analyzing fracture aperture evolution in our experiments.

Some parameters, such as plasticity index, clay content, liquid index, and liquid limit, affect the swelling effect of clay minerals [29–32]. Besides, simulation methods showed under high fluid acidic conditions, clay swelling effect is much smaller than low fluid acidic and alkaline conditions will increase the negative charges in clay surface and further increase the potential of clay swelling which referred as alkali-sensitive damage in oil formation [33].

One limitation of our research is that we cannot quantitatively constrain the fracture aperture changing rate with time from the respective of pore volume change for clay mineral swell. Hence, fitting method based on contemporary experimental results is used. As shown in Figure 13,

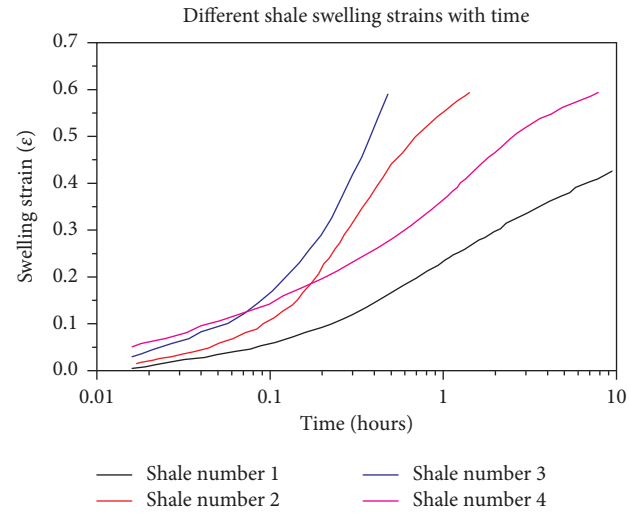


Figure 13: The relationship between swelling strain and time for four different kinds of shale (modified from reference [32]). The swelling speed decreases largely with time.

Table 3: The fitting results between swell strain and time.

| Shale number | Fitting equation | Coefficient of determination |
|---|---|---|
| 1 | $\varepsilon_{\text{swell}} = 0.0718\times\ln(t) - 0.0520$ | 0.966 |
| 2 | $\varepsilon_{\text{swell}} = 0.1466\times\ln(t) - 0.0908$ | 0.936 |
| 3 | $\varepsilon_{\text{swell}} = 0.1535\times\ln(t) - 0.0412$ | 0.902 |
| 4 | $\varepsilon_{\text{swell}} = 0.0953\times\ln(t) - 0.0028$ | 0.975 |

Chenevert conducted experiments on different shale to constrain the relationship between time and swelling strain [32]. Results showed that swelling almost happens in the first 1 or 2 hours, and swelling speed decreases dramatically with time. Those data are used to constrain the relationship between time and swell, and fitting results are shown in Table 3.

The relation between swell strain ($\varepsilon_{\text{swell}}$) and time ($t$) could be described as the following form:

$$\varepsilon_{\text{swell}} = a\ln(t) + b, \tag{12}$$

where $a$ and $b$ are fitting parameters.

Furthermore, the fracture aperture evolution with time solely by clay swell could be estimated as

$$\begin{aligned} e &= e_{\text{initial}} - D\cdot\varepsilon_{\text{swell}} \\ &= e_{\text{initial}} - D\cdot(a\ln(t)+b) \\ &= -a\cdot D\ln(t) + (e_{\text{initial}} - b\cdot D), \end{aligned} \tag{13}$$

where $e_{\text{initial}}$ is initial aperture, and $D$ is sample diameter. The decrease rate with time could be calculated as

$$\frac{d\varepsilon_{\text{swell}}}{dt} = -\frac{d(D\cdot\varepsilon_{\text{swell}})}{dt} = D\cdot\frac{d\varepsilon_{\text{swell}}}{dt} = D\cdot\frac{a}{t}. \tag{14}$$

Table 4: Predicted Marcellus shale aperture evolution.

| Fluid pH | Fitting equation | Fitted $m$ | Coefficient of determination |
|---|---|---|---|
| 4.0 | $e = 30.56521 - 2.32846 \ln(t)$ | −2.328 | 0.906 |
| 5.0 | $e = 30.02814 - 2.54101 \ln(t)$ | −2.541 | 0.916 |
| 6.0 | $e = 29.95431 - 3.00063 \ln(t)$ | −3.001 | 0.892 |
| 7.0 | $e = 29.95995 - 3.14536 \ln(t)$ | −3.145 | 0.945 |

Hence, the fracture aperture decrease rate caused by clay swell could be expressed as

$$\frac{de_{\text{swell}}}{dt} = \frac{m}{t}, \tag{15}$$

where $m$ is a clay swelling-related parameter which controlled by plasticity index (PI), clay content, liquid index, liquid limit, and plasticity index and could be estimated from experimental results.

Now, the multiple parameter model which considers calcite pressure solution, free-face dissolution, and clay swell effect on fracture aperture change is built in shale, which is

$$e_{\text{h}} = e_{\text{initial}} - \left[\frac{3V_{\text{m}}^2}{RT}(1 - R_{\text{c}})\left(\frac{\sigma_{\text{conf}}}{R_{\text{c}}} - \sigma_{\text{c}}\right) \times k_1\right] \times t + 2(1 - R_{\text{c}}) \times V_{\text{m}} k_2 \times t + m \times \ln(t). \tag{16}$$

## 5. Discussion

In this part, the multiple parameter model is deployed to calculate the fracture aperture evolution for different shale under various combinations of confining stress, inlet fluid acidity, and shale mineralogy. As the length limit, the detailed methods to determine critical parameter dissolution rate ($k_1$, $k_2$) and contact area ratio ($R_{\text{c}}$) are presented in Supplementary Materials (A1 and A2 sections).

*5.1. Fracture Aperture Evolution in Shale without Calcite.* For Marcellus shale, the only mechanism controlling aperture evolution is clay swelling due to the absence of calcite mineral. The detailed discussion is presented in A3 section in Supplementary Materials. Hence, (16) is simplified as

$$e_{\text{h}} = e_{\text{initial}} + m \times \ln(t). \tag{17}$$

The aperture changing rate is described, and $m$ is estimated based on experimental data under different acidic conditions. The results are summarized in Table 4.

The fitting results in Table 4 indicate that this model could effectively predict the Marcellus shale fracture aperture evolution.

*5.2. Fracture Aperture Evolution in Shale with Calcite.* For Longmaxi shale and Green River shale, where calcite pressure solution, free-face dissolution, and clay swell happen simultaneously, the permeability evolution is complicated and analyzed as below.

(1) Fluid pH = 6.0 and 7.0: when fluid pH = 7.0 and 6.0, the fracture aperture evolution decreases. Equation (16) could be simplified as

$$e_{\text{h}} = e_{\text{initial}} + a \cdot t - m \ln(t). \tag{18}$$

In (18), $a$ is the parameter describing the fracture aperture change due to free-face dissolution and pressure solution, and $m$ is the parameter characterizing the fracture aperture evolution caused by clay swell. Parameter $a$ could be derived from (16) as

$$a = -\frac{3V_{\text{m}}^2}{RT}(1 - R_{\text{c}})\left(\frac{\sigma_{\text{conf}}}{R_{\text{c}}} - \sigma_{\text{c}}\right) \cdot k_1 + 2(1 - R_{\text{c}}) \cdot V_{\text{m}} k_2. \tag{19}$$

Hence, after data fitting, fracture effective hydraulic aperture evolution when fluid pH = 6.0 and 7.0 is summarized in Table 5.

(2) Fluid pH = 4.0 and 5.0: the priority thing is to decide the critical point which we observed during core flooding experiments under pH = 4.0 and 5.0 condition, where fracture aperture evolution transferred from aperture gaping to aperture closing.

SEM-EDS results showed that after core flooding experiments of pH = 4.0 and 5.0 fluid, Ca mass fraction in fracture surface is less than 1% in Longmaxi shale. Even the Ca fraction is almost 9% after core flooding tests. The reason could be the high dolomite percentage in Green River shale, which is 39.0% before core flooding tests. As shown in Table 6, the dissolution rate of calcite and dolomite is summarized, which indicates that dissolution rate of calcite is 10~100 times larger than dolomite dissolution rate under the same fluid acidity. It should be noted that the detailed method for calcite dissolution rate could be found in Appendix A1, and dolomite dissolution rate data are recovered from [34]. Hence, the critical points occur when the fracture surface calcite content is almost zero where Ca could still exist as the form of dolomite which has a really low dissolution rate with carbonic acid. Hence, before critical point, competing roles among calcite free-face dissolution, pressure solution, and clay swell gaping the fracture aperture and after that calcite disappeared and its free-face dissolution ceased and quartz pressure solution becomes the dominant mechanism to close the fracture aperture.

In the fracture gaping period, almost linear increase is observed for Longmaxi shale and Green River shale while consistent decrease is observed for Marcellus shale. Different from Marcellus shale where kaolinite is the main clay swell who has a larger swell potential, the main clay mineral in Longmaxi shale and Green River shale is illite, which is always been regarded as unswell clay. Hence, the clay swell effect is neglected which is much smaller compared with

Table 5: Predicted Longmaxi shale and Green River shale aperture evolution (pH = 6.0 and 7.0).

| Shale | Fluid pH | Confining stress | Fitting equation | Coefficient of determination |
|---|---|---|---|---|
| Longmaxi | 7.0 | 3.0 | $e_h = 31.91896 - 0.80179\ln(t) - 0.0003757.7 \times t$ | 0.911 |
| | 7.0 | 5.0 | $e_h = 31.44867 - 1.06542\ln(t) - 0.001165378 \times t$ | 0.937 |
| | 7.0 | 10.0 | $e_h = 22.18106 - 0.72442\ln(t) - 0.002677789 \times t$ | 0.956 |
| | 6.0 | 3.0 | $e_h = 31.54955 - 0.65021\ln(t) + 0.00123713 \times t$ | 0.841 |
| | 6.0 | 5.0 | $e_h = 26.56389 - 0.60462\ln(t) + 0.000415405 \times t$ | 0.872 |
| | 6.0 | 10.0 | $e_h = 21.84205 - 0.13463\ln(t) - 0.001156053 \times t$ | 0.929 |
| Green River | 7.0 | 10.0 | $e_h = 26.86063 - 0.50583\ln(t) - 0.001156053 \times t$ | 0.784 |
| | 6.0 | 10.0 | $e_h = 25.25844 - 0.20519\ln(t) - 0.0017078 \times t$ | 0.877 |

Table 6: Comparison of dissolution rate of calcite and dolomite under various fluid acidities.

| Fluid pH | Calcite dissolution rate (mol/m$^2$ s) | Dolomite dissolution rate (mol/m$^2$ s) |
|---|---|---|
| 4.0 | $9.23 \times 10^{-5}$ | $3.31 \times 10^{-7}$ |
| 5.0 | $9.55 \times 10^{-6}$ | $1.38 \times 10^{-7}$ |
| 6.0 | $1.12 \times 10^{-6}$ | $2.95 \times 10^{-8}$ |
| 7.0 | $7.39 \times 10^{-7}$ | $3.09 \times 10^{-8}$ |

fracture aperture gap caused by calcite free-face dissolution. Thus, (16) is simplified as

$$e_h = e_{initial} + a \cdot t. \tag{20}$$

The calculated $a$ value and observed aperture increase rate are summarized in Table 7.

After calculation, the observed fracture aperture increase rate cannot reach the predicted one. The reason could be the $k_2$ value selection. As mentioned before, the $k_2$ value is the calcite dissolution rate in free-face area. In Supplementary Materials, Table A1, the dissolution rate of calcite is measured under static condition which means fluid keeps stable during experiments. However, in our core flooding experiment, even though the certain pH fluid is injected continuously, if the flow rate is small, the later area could not get as lower as fluid pH in inlet area.

Besides that, some other factors could affect the calcite dissolution rate including calcite grains size, crystallinity, impurities, and defect density. In our shale samples, the mutual effect of quartz and calcite in mineral structure could also lower the calcite dissolution rate due to calcite could be covered partially by quartz or some other inactive minerals.

As for the fracture aperture decrease period, after calcite mineral disappears in fracture surface in Longmaxi and Green River shale, the quartz becomes the dominant mineral and its pressure solution leads to a monotonically decrease of fracture aperture, since the dissolution rate for quartz is $2.51 \times 10^{-9}$ mol/m$^2$ s under neutral condition (pH = 7), which leads to a fracture aperture decrease rate ~ $10^{-6}$ $\mu$m/h and it could be neglected. This calculation result is in accordance with experimental observations that after calcite disappeared in fracture surface, the fracture aperture keeps at a relative stable state.

*5.3. Discussion on Multiple Parameter Model.* Modified from (16), the effective hydraulic aperture changing rate is expressed as

$$\frac{de_h}{dt} = -\frac{3V_m^2}{RT}(1 - R_c)\left(\frac{\sigma_{conf}}{R_c} - \sigma_c\right) \cdot k_1 + 2(1 - R_c) \cdot V_m k_2 + \frac{m}{t}. \tag{21}$$

Based on (21), some basic understandings are drawn as follows:

(1) Pressure solution-induced fracture aperture decrease is constant during fracture closing process, which is only controlled by effective stress and isolated with fluid acidity. The relationship between fracture closing rate and confining stress is plotted in Figure 14.

In Figure 14, even if the effective stress reaches 100 MPa, the fracture closing rate is only 1.19 $\mu$m/h. That is the reason in some research that the pressure solution cannot be observed since initial fracture aperture is as large as several hundred microns [35]. Hence, on the conditions when effective stress is large enough which makes initial fracture aperture is relative small and fracture aperture closing rate induced solely by pressure solution is large, mineral pressure solution plays an important role in determining permeability evolution.

(2) When injecting acidic fluid, free-face dissolution-induced fracture permeability increase is the most important mechanism to gap the fracture. The increasing rate is controlled by fluid acidity and calcite dissolution rate. The relationship between fracture increasing rate caused by free-face dissolution and fluid acidity is plotted in Figure 15.

As shown in Figure 15, fracture effective hydraulic aperture gaping rate reaches ~20 $\mu$m/h when fluid pH = 4.0, which is almost 20 times larger than decreasing rate caused by calcite pressure solution effect. With the decrease of fluid

Table 7: Predicted versus observed effective hydraulic aperture increase for Longmaxi shale and Green River shale (pH = 4.0 and 5.0).

| Shale name | Fluid pH | Confining stress (MPa) | Calculated ($\mu$m/min) | Observed ($\mu$m/min) | Relative error (%) | Corresponding $k_2$ (mol/m$^2$ s) |
|---|---|---|---|---|---|---|
| Longmaxi | 4.0 | 3.0 | 0.3872 | 0.1811 | −53.23 | $4.36 \times 10^{-5}$ |
| | 4.0 | 5.0 | 0.3787 | 0.1420 | −62.51 | $3.52 \times 10^{-5}$ |
| | 4.0 | 10.0 | 0.3630 | 0.1496 | −58.79 | $3.89 \times 10^{-5}$ |
| | 5.0 | 3.0 | 0.0369 | 0.0195 | −47.19 | $5.47 \times 10^{-6}$ |
| | 5.0 | 5.0 | 0.0354 | 0.0085 | −75.98 | $3.08 \times 10^{-6}$ |
| | 5.0 | 10.0 | 0.0325 | 0.0055 | −83.08 | $2.79 \times 10^{-6}$ |
| Green River | 4.0 | 10.0 | 0.3653 | 0.1106 | −69.72 | $2.91 \times 10^{-5}$ |
| | 5.0 | 10.0 | 0.0322 | 0.0305 | −5.35 | $9.12 \times 10^{-6}$ |

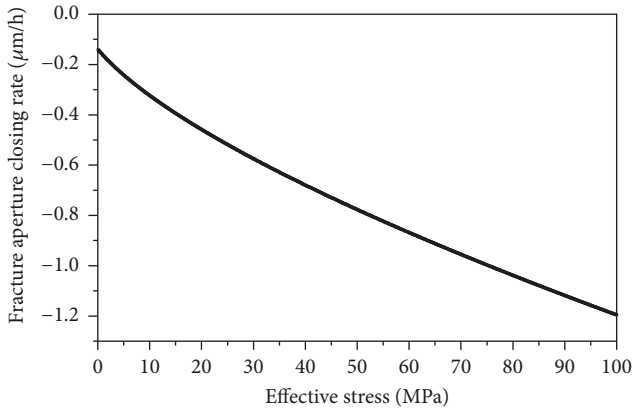


Figure 14: The relationship between fracture closing rate and confining stress.

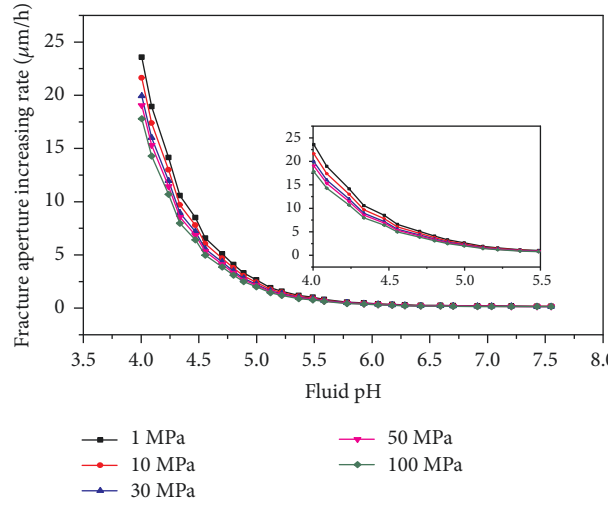


Figure 15: The relationship between fracture increasing rate and fluid acidity caused by calcite free-face dissolution.

acidity, fracture effective hydraulic aperture increasing rate decreases dramatically.

(3) The clay mineral swell cannot be neglected during permeability evolution in shale, especially for shale with high-potential clay mineral montmorillonite. The clay swelling-induced fracture permeability decrease always happens in the first one or two hours, due to the reason that clay swell strain speed decreases largely with time.

As a summary, the effective hydraulic aperture evolution with time under various conditions is summarized in Figure 16.

As shown in Figure 16, a complex and enigmatic fashion is observed for effective hydraulic aperture evolution under various combinations of shale mineral compositions, fluid acidity, and effective stress. (a) For shale with calcite under high fluid acidic conditions, calcite free-face dissolution dominates over pressure solution due to the larger dissolution rate in noncontacting areas than contacting asperities, which gap the fracture aperture and then keep a relative stable state where quartz pressure solution dominates fracture aperture evolution due to the extremely low dissolution rate of quartz. (b) For shale with calcite under low fluid acidic conditions, phase I—calcite pressure solution and clay swell decrease fracture aperture; phase II—clay swell terminates and calcite pressure solution decreases fracture aperture; phase III—calcite pressure solution terminates and quartz pressure solution closes fractures at an extreme low rate. (c) For shale with high clay content, clay swell closes fracture aperture and higher fluid acidity depresses changing rate.

## 6. Conclusions

In summary, $CO_2$-rich aqueous fluids have significant impact on the evolution of fracture permeability and may increase shale gas production. Experimental observations and theoretical analysis are combined to build a multiple parameter model to describe fracture effective hydraulic aperture evolution under various combinations of fluid acidity, effective stress, and shale mineralogy. The main conclusions are drawn as follows:

(1) Shale mineralogy, especially calcite mineral, decides the chemical reaction and permeability increasing when $CO_2$-rich aqueous fluids flow through; calcite free-face dissolution is the main reason which contributes to fracture permeability increase and higher acidity fluid leads to a larger fracture aperture increase.

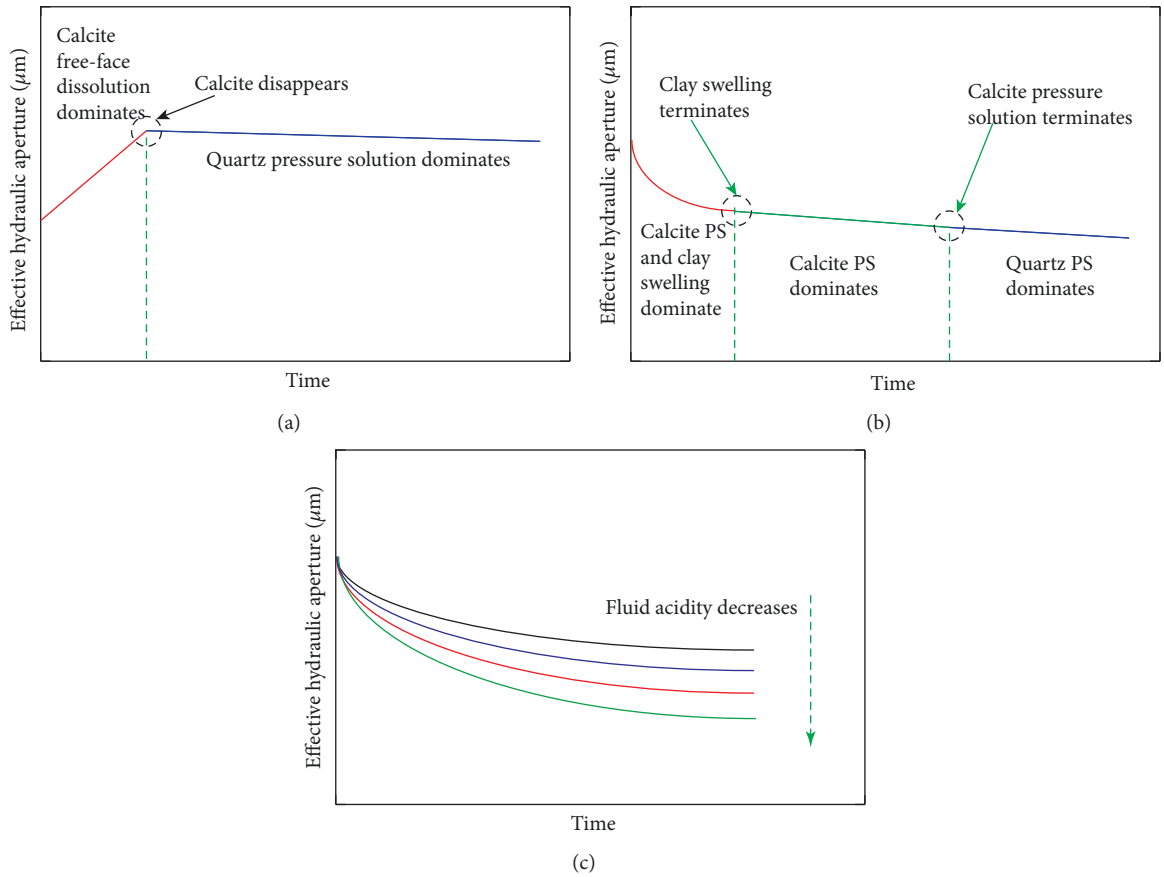


Figure 16: Effective hydraulic aperture evolution with time under various conditions in shale. (a) Shale with calcite under high fluid acidity conditions, (b) shale with calcite under low fluid acidity conditions, and (c) shale with high clay content.

(2) Calcite pressure solution removes the bridging asperities in contacting areas, which are the main reasons for fracture permeability decrease when the fluids flow through. In addition, pressure solution-induced fracture aperture decrease rate is constant during fracture closing process, which is only controlled by effective stress and isolated with fluid acidity.

(3) Clay mineral, especially montmorillonite, swelling reduces fracture permeability largely in the first one or two hours, due to the reason that clay swell strain speed deceases largely with time.

(4) Those three effects operate in different and complex ways, and competition roles among them determine whether fracture permeability increases or decreases; the multiple parameter model built in this paper is an effective method to predict fracture permeability evolution in shale considering the above three mechanisms when choosing appropriate parameters.

## Data Availability

The data used to support the findings of this study are plotted within the article, and the raw data files are available by contacting the first author at cqujyz@gmail.com.

## Conflicts of Interest

The authors declare that they have no conflicts of interest.

## Acknowledgments

The authors thank Derek Elsworth (Penn State University, USA) for designing the experiment and Hideaki Yasuhara (Ehime University, Japan) for his advice in constraining the relationship between contact area ratio and effective stress. Discussion with Xiaohong Li (Chongqing University, China), Takuya Ishibashi (National Institute of Advanced Industrial Science and Technology, Japan), and Chaoyi Wang (Penn State University, USA) also helps to improve the manuscript. This work is the partial result of support provided by the National Key Basic Research Program of China (Grant no. 2014CB239206), the Major Research Plan of the National Science and Technology in 13th Five-Year Plan (no.2017ZX05049-003-11), and the Program for Changjiang Scholars and Innovative Research Team in Chongqing University (Grant no. IRT17R112).

## Supplementary Materials

A1: determination of calcite dissolution rate $k_1$, $k_2$. A2: determination of relationship between contact area ratio ($R_c$) and confining stress. A3: the simplification process from (16) to

(17). The supplementary material helps readers understand our model easily and further apply similar methods in their relevant researches. *(Supplementary Materials)*

## References


[1] Y. Jia, Y. Lu, D. Elsworth, Y. Fang, and J. Tang, "Surface characteristics and permeability enhancement of shale fractures due to water and supercritical carbon dioxide fracturing," *Journal of Petroleum Science & Engineering*, vol. 165, pp. 284–297, 2018.

[2] X. Zhang, Y. Lu, J. Tang, Z. Zhou, and Y. Liao, "Experimental study on fracture initiation and propagation in shale using supercritical carbon dioxide fracturing," *Fuel*, vol. 190, pp. 370–378, 2016.

[3] T. Ishida, Y. Chen, Z. Bennour et al., "Features of $CO_2$ fracturing deduced from acoustic emission and microscopy in laboratory experiments," *Journal of Geophysical Research Solid Earth*, vol. 121, no. 11, pp. 8080–8098, 2016.

[4] J. Wang, D. Elsworth, Y. Wu, J. Liu, W. Zhu, and Y. Liu, "The influence of fracturing fluids on fracturing processes: a comparison between water, oil and SC-$CO_2$," *Rock Mechanics and Rock Engineering*, vol. 51, no. 1, pp. 299–313, 2018.

[5] B. R. Scanlon, R. C. Reedy, and J. P. Nicot, "Response to comment on "comparison of water use for hydraulic fracturing for unconventional oil and gas versus conventional oil"," *Environmental Science & Technology*, vol. 49, no. 10, pp. 6358-6359, 2015.

[6] P. Gouze, C. Noiriel, C. Bruderer, D. Loggia, and R. Leprovost, "X-ray tomography characterization of fracture surfaces during dissolution," *Geophysical Research Letters*, vol. 30, no. 5, pp. 225–242, 2003.

[7] C. Noiriel, B. Madé, and P. Gouze, "Impact of coating development on the hydraulic and transport properties in argillaceous limestone fracture," *Water Resources Research*, vol. 43, no. 9, pp. 2363–2367, 2007.

[8] P. Cao, Z. T. Karpyn, and L. Li, "Dynamic alterations in wellbore cement integrity due to geochemical reactions in $CO_2$-rich environments," *Water Resources Research*, vol. 49, no. 7, pp. 4465–4475, 2013.

[9] G. Izadi and D. Elsworth, "The influence of thermal-hydraulic-mechanical- and chemical effects on the evolution of permeability, seismicity and heat production in geothermal reservoirs," *Geothermics*, vol. 53, pp. 385–395, 2015.

[10] H. Yasuhara, D. Elsworth, and A. Polak, "Evolution of permeability in a natural fracture: significant role of pressure solution," *Journal of Geophysical Research: Solid Earth*, vol. 109, article B03204, 2004.

[11] A. Polak, D. Elsworth, H. Yasuhara, A. S. Grader, and P. M. Halleck, "Permeability reduction of a natural fracture under net dissolution by hydrothermal fluids," *Geophysical Research Letters*, vol. 30, no. 20, article 2020, 2003.

[12] J. Taron and D. Elsworth, "Constraints on compaction rate and equilibrium in the pressure solution creep of quartz aggregates and fractures: controls of aqueous concentration," *Journal of Geophysical Research: Solid Earth*, vol. 115, no. B7, 2010.

[13] R. L. Detwiler, "Permeability alteration due to mineral dissolution in partially saturated fractures," *Journal of Geophysical Research Solid Earth*, vol. 115, no. B9, 2010.

[14] P. Szymczak and A. J. C. Ladd, "Microscopic simulations of fracture dissolution," *Geophysical Research Letters*, vol. 31, no. 23, pp. 275–295, 2011.

[15] H. Yasuhara, A. Polak, Y. Mitani, A. S. Grader, P. M. Halleck, and D. Elsworth, "Evolution of fracture permeability through fluid–rock reaction under hydrothermal conditions," *Earth and Planetary Science Letters*, vol. 244, no. 1-2, pp. 186–200, 2006.

[16] T. P. Mcguire, D. Elsworth, and Z. Karcz, "Experimental measurements of stress and chemical controls on the evolution of fracture permeability," *Transport in Porous Media*, vol. 98, no. 1, pp. 15–34, 2013.

[17] T. Ishibashi, T. P. Mcguire, N. Watanabe, N. Tsuchiya, and D. Elsworth, "Permeability evolution in carbonate fractures: competing roles of confining stress and fluid ph," *Water Resources Research*, vol. 49, no. 5, pp. 2828–2842, 2013.

[18] I. Faoro, S. Vinciguerra, C. Marone, D. Elsworth, and A. Schubnel, "Linking permeability to crack density evolution in thermally stressed rocks under cyclic loading," *Geophysical Research Letters*, vol. 40, no. 11, pp. 2590–2595, 2013.

[19] Y. Lu, X. Ao, J. Tang, Y. Jia, X. Zhang, and Y. Chen, "Swelling of shale in supercritical carbon dioxide," *Journal of Natural Gas Science & Engineering*, vol. 30, no. 4, pp. 268–275, 2016.

[20] Y. Fang, D. Elsworth, C. Wang, T. Ishibashi, and J. P. Fitts, "Frictional stability-permeability relationships for fractures in shales," *Journal of Geophysical Research Solid Earth*, vol. 122, no. 3, pp. 1760–1776, 2017.

[21] I. Palmer, Z. Moschovidis, and J. Cameron, "Modeling shear failure and stimulation of the Barnett Shale after hydraulic fracturing," in *SPE Hydraulic Fracturing Technology Conference*, College Station, TX, USA, January 2007.

[22] A. Polak, D. Elsworth, J. Liu, and A. S. Grader, "Spontaneous switching of permeability changes in a limestone fracture with net dissolution," *Water Resources Research*, vol. 40, no. 3, pp. 383–391, 2004.

[23] M. Manga, I. Beresnev, E. E. Brodsky et al., "Changes in permeability caused by transient stresses: field observations, experiments, and mechanisms," *Reviews of Geophysics*, vol. 50, no. 2, 2012.

[24] D. Elsworth and H. Yasuhara, "Short-timescale chemo-mechanical effects and their influence on the transport properties of fractured rock," *Pure and Applied Geophysics*, vol. 163, no. 10, pp. 2051–2070, 2006.

[25] L. P. Stephenson, W. J. Plumley, and V. V. Palciauskas, "A model for sandstone compaction by grain interpenetration," *SPE Hydraulic Fracturing Technology Conference*, vol. 62, 1992.

[26] W. Dreybrodt and D. Buhmann, "A mass transfer model for dissolution and precipitation of calcite from solutions in turbulent motion," *Chemical Geology*, vol. 90, no. 1-2, pp. 107–122, 1991.

[27] I. Aksu, E. Bazilevskaya, and Z. T. Karpyn, "Swelling of clay minerals in unconsolidated porous media and its impact on permeability," *Georesj*, vol. 7, pp. 1–13, 2015.

[28] A. Sanaei, M. Shakiba, A. Varavei, and K. Sepehrnoori, "Mechanistic modeling of clay swelling in hydraulic-fractures network," *SPE Reservoir Evaluation & Engineering*, vol. 21, no. 1, pp. 96–108, 2016.

[29] Z. A. Erguler and R. Ulusay, "A simple test and predictive models for assessing swell potential of Ankara (Turkey) clay," *Engineering Geology*, vol. 67, no. 3-4, pp. 331–352, 2003.

[30] E. T. Selig, L. D. Johnson, and D. R. Snethen, "Prediction of potential heave of swelling soil," *Geotechnical Testing Journal*, vol. 1, no. 3, pp. 117–124, 1978.

[31] M. Muthukumar and S. K. Shukla, "Swelling behaviour of expansive clay beds reinforced with encased granular pile anchors," *International Journal of Geotechnical Engineering*, vol. 12, no. 2, pp. 109–117, 2016.

[32] M. E. Chenevert, "Shale alteration by water adsorption," *Journal of Petroleum Technology*, vol. 22, no. 9, pp. 1141–1148, 1970.

[33] W. Fang, H. Jiang, J. Li et al., "A new experimental methodology to investigate formation damage in clay-bearing reservoirs," *Journal of Petroleum Science & Engineering*, vol. 143, pp. 226–234, 2016.

[34] O. S. Pokrovsky, S. V. Golubev, and J. Schott, "Dissolution kinetics of calcite, dolomite and magnesite at 25°C and 0 to 50 atm $pCO_2$," *Chemical Geology*, vol. 217, no. 3-4, pp. 239–255, 2005.

[35] H. Deng, B. R. Ellis, C. A. Peters, J. P. Fitts, D. Crandall, and G. S. Bromhal, "Modifications of carbonate fracture hydrodynamic properties by $CO_2$-acidified brine flow," *Energy & Fuels*, vol. 27, no. 8, pp. 4221–4231, 2013.